

Cite this: *Soft Matter*, 2011, **7**, 5777

www.rsc.org/softmatter

PAPER

# An alternative route to highly concentrated, freely flowing colloidal dispersions

Norbert Willenbacher,<sup>\*a</sup> Jan S. Vesaratchanon,<sup>a</sup> Otilie Thorwarth<sup>b</sup> and Eckhard Bartsch<sup>b</sup>

Received 7th February 2011, Accepted 6th April 2011

DOI: 10.1039/c1sm05200d

Dense colloidal dispersions exhibit fluid states due to weak attractive interactions among particles even at particle volume fractions far above the colloidal glass transition. Here we demonstrate that this opens up a new route to manufacture highly concentrated, freely flowing dispersions. We have studied the rheological properties of two model dispersions in the dense, fluid state: PS-microgel particles suspended in an isorefractive organic solvent allowing for light scattering experiments and an aqueous polymer latex dispersion with short range repulsive interactions based on a commercial polymer latex system. Both systems essentially behave like hard spheres, their zero-shear viscosity diverges at a volume fraction  $\phi = 0.58$ , linear viscoelastic behavior is well-described by the mode coupling theory and the absolute values of the plateau moduli are close to those reported for other hard sphere systems. Fluidization was achieved by introducing weak depletion attraction among particles *via* addition of non-adsorbing polymers to the continuous phase. Fluid states were observed up to  $\phi \approx 0.69$  for the microgel and  $\phi \approx 0.644$  for the aqueous system. At a given particle loading a minimum viscosity was achieved at polymer concentrations below the overlap concentration  $c_p^*$ . For the aqueous dispersion fluidization was observed for a broad range of polymer molecular weights  $M_w$  and the respective viscosity minimum did not vary systematically with  $M_w$ . The low viscosity values thus achieved for nearly monomodal systems could so far only be obtained for dispersions with broad multimodal particle size distribution, demonstrating the competitive nature of the new concept.

## 1. Introduction

Colloidal dispersions are encountered in many traditional applications, including paints, inks, cosmetics, pharmaceuticals or foods.<sup>1</sup> Nowadays, colloid science and technology also play a key role in emerging technologies such as tissue engineering scaffolding,<sup>2</sup> photonic crystals,<sup>3</sup> 3D ink-jet technology,<sup>4</sup> advanced ceramics processing<sup>5</sup> or microfluidics.<sup>6</sup> A key technological challenge in designing such materials is to control their flow properties in order to meet the manifold requirements during processing and application. This topic is especially relevant when dealing with nanoparticle formulations on a technical scale where high particle loadings are required. Making highly concentrated dispersions is a persistent challenge since it allows for higher time-space yield during manufacturing, reduced transport costs and drying energy particularly in large scale industrial coating applications, and also provides additional degrees of freedom in formulation of complex fluids.

The classical route to achieve high particle loading at low viscosity level in suspensions is to provide a bimodal or broad particle size distribution.<sup>7,8</sup> This is not always technically or economically feasible and large particles may disturb final product properties. In colloidal systems viscosity reduction is limited due to interactions among particles, which get increasingly relevant as particle size decreases. For bimodal dispersions a minimum viscosity is reached at a fraction of small particles of about 30% and a size ratio  $\sigma \approx 4$ –5.<sup>9,10</sup> Here we present an alternative concept to make highly concentrated, freely flowing dispersions, based on the so-called re-entry glass transition in colloidal dispersions which has been predicted theoretically<sup>11–13</sup> and confirmed experimentally for various model dispersions.<sup>14–20</sup> Weak attractive interactions are supposed to lead to reversible particle clustering, which opens up the space allowing for long-range particle motion and macroscopic flow, thus melting the glassy state. We demonstrate that monomodal dispersions with particle loadings up to  $\phi \approx 0.7$  can be fluidized and that the viscosity can be reduced to the level of commercial dispersions with broad particle size distribution in a wide shear rate range representing essential manufacturing and processing conditions.

Phase behavior,<sup>21</sup> dynamics and flow of colloidal dispersions are strongly controlled by particle volume fraction  $\phi$ .<sup>22</sup> Progressive crowding eventually leads to a vitrification when

<sup>a</sup>Karlsruhe Institute of Technology, Institute of Mechanical Process Engineering and Mechanics, Karlsruhe, Germany. E-mail: Norbert.Willenbacher@kit.edu

<sup>b</sup>University of Freiburg, Institute of Physical Chemistry, Freiburg, Germany. E-mail: Eckhard.Bartsch@physchem.uni-freiburg.de

particles are trapped within a virtual cage provided by nearest neighbors. Long range particle motion slows down and the low shear viscosity diverges when a critical concentration  $\phi_g$ , the glass transition, is approached,<sup>23</sup> a finite zero-frequency modulus  $G_0$  is observed beyond  $\phi_g$ . The mode coupling theory (MCT) has been successfully employed to describe this phenomenon.<sup>24–26</sup> Barrat *et al.* have predicted a critical scaling exponent for the divergence of the zero-shear viscosity,<sup>27</sup> Nägele and Bergenholtz have developed a general method to describe the linear viscoelastic properties,<sup>28</sup> Fuchs and Cates<sup>29,30</sup> have generalized the MCT to treat the non-linear dynamics of colloidal suspension in shear flow and careful experiments on well-characterized model systems have confirmed that flow curves are predicted very well by the MCT in a wide shear rate range.<sup>31,32</sup>

The MCT also predicts that two different glassy states exist in dispersions of particles with weak short-range attraction, one due to particle caging (repulsive glass), the other due to particle bonding (attractive glass) and the glass transition is shifted to a higher  $\phi$ .<sup>11–13,33</sup> This has been confirmed experimentally for different colloidal dispersions, namely PMMA particles<sup>14,15</sup> and PS-microgel particles<sup>16–18</sup> suspended in an isorefractive organic solvent. In both cases attractive depletion interactions were introduced by addition of non-adsorbing polystyrene (PS) molecules to the continuous phase of the dispersion. Phase diagrams were obtained from dynamic light scattering experiments and the transition from ergodic to the non-ergodic, glassy state was identified by the non-vanishing long-time limit of the dynamic structure factor  $f(q, \tau \rightarrow \infty) > 0$ . The phase diagrams show a significant curvature of the fluid–glass transition line and at a fixed particle loading a transition from the glassy to the fluid state and then again from the fluid to the attractive glassy state is observed when the polymer concentration and hence the strength of attractive interaction is increased (re-entry glass transition). Fluid states were observed up to  $\phi \approx 0.61$  for the PMMA system and  $\phi \approx 0.68$  for the PS-microgel system.

Up to now little is known about the consequences of the re-entry phenomenon for the macroscopic flow behavior. The effect of depletion attraction on the rheology and on the viscoelasticity of nearly hard sphere silica particles suspended in decalin or toluene has been investigated carefully<sup>19,20</sup> and a minimum of the low shear viscosity as a function of polymer concentration has been observed.<sup>34,35</sup> The zero shear viscosity is reduced by a factor of three at a particle volume fraction  $\phi = 0.49$ , a polymer to particle size ratio of  $R_g/R = 0.05$  and a polymer concentration  $c_p/c_p^* = 0.03$  well below the overlap concentration  $c_p^*$ . This clearly demonstrates that weak attractive particle interactions can lead to a significant decrease of the viscosity compared to hard sphere systems or even systems with strong repulsive or attractive interactions. However, it should be noted that in this case the particle volume fraction is still below the hard sphere glass transition. Another example has been reported by Pham *et al.*,<sup>36</sup> who observed a reduction of the storage modulus  $G'$  by a factor of three for a system of sterically stabilized polymethylmethacrylate (PMMA) particles ( $R = 130$  nm) suspended in decalin at a particle volume fraction  $\phi = 0.6$  and a polymer concentration of  $c_p/c_p^* = 0.15$ . This shows that weak attractions among colloidal particles in suspension can alter macroscopic rheological quantities even in the particle concentration range above the hard sphere glass

transition. On the other hand, from a technical point of view the rheological effects observed so far may be too small to be of significant technical relevance. Moreover, the re-entry phenomenon has not been investigated so far for aqueous suspensions, which are of paramount importance from a technical point of view. The fluidization reported for flocculated, nearly hard sphere aqueous silica suspensions<sup>37</sup> upon addition of a small fraction of highly charged nanoparticles (size ratio  $\leq 0.01$ ) is an electrostatically driven phenomenon and, therefore, different in nature from the re-entry phenomenon considered here, although an attractive glass forms again, when the nanoparticle concentration is further increased. This depletion induced flocculation of aqueous colloidal suspensions is well documented in the literature.<sup>38,39</sup>

In this contribution we discuss the re-entry phenomenon from a rheological point of view for microgel systems similar to the one used earlier<sup>16</sup> and we demonstrate that the small fraction of slightly larger particles included in these microgel mixtures in order to slow down crystallization is rheologically not significant. Furthermore, we demonstrate that the re-entry phenomenon can be observed for aqueous colloidal suspensions of polymer particles with short range electrosteric repulsion. The aqueous system is based on a commercial dispersion with fairly narrow particle size distribution.<sup>40</sup> The suspensions and the methods are described in section two, results are presented and discussed in section three and finally conclusions are drawn and the technical impact is discussed in comparison with the generally used concept of viscosity reduction due to a broad multimodal particle size distribution.

## 2. Experimental

### Materials and methods

**PS-microgels.** Two batches of polystyrene (PS) microgels particles with a crosslink density 1 : 50 have been synthesized by emulsion polymerization, purified and dried as described previously.<sup>41</sup> Particle sizes in aqueous dispersion as determined by dynamic light scattering (DLS) were  $R_{h,H_2O} = 80 \pm 2$  nm and  $R_{h,H_2O} = 113 \pm 2$  nm, respectively. The particle size in vacuum dried state and the polydispersity, *i.e.* the normalized standard deviation,  $\sigma_R = (\langle R^2 \rangle - \langle R \rangle^2)^{1/2} / \langle R \rangle$ , were obtained by transmission electron microscopy (TEM) providing  $R_{TEM} = 79 \pm 3$  nm ( $\sigma_R = 0.032$ ) and  $R_{TEM} = 105 \pm 3$  nm ( $\sigma_R = 0.02$ ), respectively. Suspended in the good, isorefractive solvent 2-ethylnaphthalene (2-EN; viscosity  $\eta_s = 0.0029$  Pa s at 293 K; refractive index<sup>17,18</sup>  $n_D = 1.599$ ) the particle size increases by a factor of  $Q^{1/3} \approx 1.8$  due to swelling in good solvents. Due to the isorefractivity of 2-EN, particle size determination *via* DLS is too inaccurate. To obtain sufficiently accurate particle radii we monitored the fluid–solid coexistence of each particle species in 2-EN and extracted the weight fractions of freezing  $w_F$  (0% crystals) and of melting  $w_M$  (100% crystals) closely following the procedure suggested by Paulin and Ackerson.<sup>42</sup> The experimental freezing point was then equated to the known freezing volume fraction of hard spheres (HS)<sup>43</sup>  $\phi_F = 0.494$  using

$$\phi = \frac{(w/d_p) \cdot Q_{HS}}{(w/d_p) + (1-w)/d_s} \quad (1)$$

where  $d_p = 1.05 \text{ g cm}^{-3}$  and  $d_s = 0.992 \text{ g cm}^{-3}$  are the mass densities of polystyrene and the solvent 2-EN, respectively. The swelling ratio  $Q_{\text{HS}}$  determined by this HS mapping was then used to obtain the effective HS particle radii *via*  $R_{\text{HS}} = Q_{\text{HS}}^{1/3} R_{\text{h,H}_2\text{O}}$ , yielding  $R_{\text{HS,S}} = 144 \pm 2 \text{ nm}$  and  $R_{\text{HS,L}} = 199 \pm 4 \text{ nm}$ , respectively (the subscripts S and L indicate small and large particles in the following). Note that the errors in the particle sizes do not enter the volume fraction determination as the latter are determined *via* eqn (1) using the  $Q_{\text{HS}}$  from hard sphere mapping. The  $Q_{\text{HS}}$  can be obtained within an accuracy of 1–2% which is then the typical error of the calculated volume fractions. The melting volume fractions  $\phi_{\text{F}}$  obtained from this procedure were  $\phi_{\text{M,S}} = 0.525 \pm 0.012$  and  $\phi_{\text{M,L}} = 0.522 \pm 0.01$ , respectively. Here, it should be noted that S and L particles were obtained in two separate synthesis batches, respectively. While the particle radii apparently are rather reproducible from batch to batch, this may not hold for the phase behaviour. Here we noted a slight, but systematic tendency of the second batch (S2,L2) towards smaller  $\phi_{\text{M}}$  values in comparison to the first batch (S1,L1), yielding  $\phi_{\text{F,S2}} = 0.519 \pm 0.007$  vs.  $\phi_{\text{F,S1}} = 0.532 \pm 0.007$  and  $\phi_{\text{F,L2}} = 0.517 \pm 0.01$  vs.  $\phi_{\text{F,L1}} = 0.527 \pm 0.01$ , respectively. Even though these differences appear to be within the experimental error, one should keep in mind that for inverse power potentials of the form  $u(r) \propto r^{-n}$  which are typically assumed for microgel particles<sup>17,42,44</sup> it is known from computer simulation that with decreasing  $n$ , *i.e.* with increasing softness of particle repulsion, the location of the freezing transition shifts to higher volume fractions and the width of the coexistence region shrinks concomitantly.<sup>45,46</sup> This behaviour has been used in the past to determine the softness exponent  $n$  for various systems.<sup>17,42,44</sup> Thus, differences in the width of the coexistence region might reflect differences in particle interaction. On the other hand, it is also known that polydispersity can have a similar effect on the coexistence region.<sup>47,48</sup> A polydispersity analysis was performed by fitting particle form factors  $P(q)$  determined *via* static light scattering (SLS) in the good solvents toluene and tetrahydrofuran (THF) with theory curves calculated for polydisperse hard spheres ( $P(q)$ s in 2-EN could not be obtained with sufficient accuracy due to the weak scattering of the particles in this iso-refractive solvent). The values  $\sigma_{\text{R}} = 0.065 \pm 0.015$  obtained have to be considered as an upper bound for the true  $\sigma_{\text{R}}$  as it is well known that SLS overestimates polydispersity due to multiple scattering effects.<sup>49,50</sup> Taking  $\sigma_{\text{R}} = 0.03$  from TEM as a lower bound a reasonable estimate for the polydispersity of the particles in swollen state is  $\sigma_{\text{R}} \approx 0.04\text{--}0.05$ . For such moderate polydispersities no significant effect on the width of the fluid–solid coexistence should be expected. To obtain information about the “particle softness” we estimated the softness exponent  $n$  of the assumed inverse power potential by determining the volume fraction dependence of the plateau modulus  $G_{\text{p}}$  *via* oscillatory shear experiments in accordance with Senff and Richtering.<sup>44</sup> For the S1 and L1 particles we find  $n = 66 \pm 5$  whereas the S2 and L2 particles yield significantly lower values of  $n = 39 \pm 5$ . These differences in particle softness are possibly due to a variation of the amount of crosslinker within the microgel particles and its spatial distribution which depends on subtle details of the synthesis protocol which are difficult to identify and to control. The observation of a more narrow fluid–solid coexistence range for the S2 and L2 particles is thus consistent with

their slightly increased softness as compared to the S1 and L1 particles. However, we do not expect these slight differences to influence significantly the particle dynamics and the flow behavior at high concentrations and the location of the glass transitions. Recently, it has been shown that for inverse power potential with  $n > 18$  that structure and dynamics of particles are identical irrespective of the  $n$ -value if the systems are compared at the same relative distance of the freezing point,<sup>51</sup> *i.e.* at the same value of  $(\phi - \phi_{\text{f}})/\phi_{\text{f}}$ . This implies that slightly soft spheres can be treated as effective hard spheres as long as an appropriate adjustment of volume fractions is performed. As this is exactly what we do by matching the freezing point of our particles to the HS value, we will in the following ignore the small differences in the interaction potentials of our particles and address them as hard spheres.

From these particles two binary HS mixtures with a size ratio  $\Gamma = R_{\text{S}}/R_{\text{L}} = 0.722 \pm 0.022$  and number ratios  $N_1 = N_{\text{S}}/N_{\text{L}} = 11$  (S1,L1) and  $N_2 = 2.5$  (S2,L2) have been prepared by weighing in the appropriate amounts of dry PS microgel and then dissolving the mixture in 2-EN. Attractive interactions among microgel particles were induced by additionally weighing in appropriate amounts of dry linear polystyrene (Polymer Standards Service GmbH, Mainz, Germany;  $M_{\text{w}} = 133\,000 \text{ g mol}^{-1}$ ,  $R_{\text{g}} = 13.1 \text{ nm}$ ,  $M_{\text{w}}/M_{\text{n}} = 1.07$ ,  $c_{\text{p}}^* = 3M_{\text{w}}/(4\pi R_{\text{g}}^3) = 23.5 \text{ g l}^{-1}$  in toluene at ambient temperature) as a non-adsorbing polymer in order to induce attractive depletion interaction among the suspended microgel particles. The volume fractions of the mixtures were then calculated according to

$$\phi = \frac{\sum_i (m_i/d_p) Q_i}{\sum_i (m_i/d_p) + (m_s/d_s)} \quad (2)$$

with the summation running over the masses  $m_i$  of all polymer components  $i = \text{S, L}$  and  $\text{p}$  ( $\text{p} = \text{free polymer}$ ) using  $Q_i = Q_{\text{HS,S}}$ ,  $Q_{\text{HS,L}}$  and 0 for components S, L and p, respectively. Here,  $m_s$  is the mass of the solvent (2-EN).

**Aqueous latex dispersions.** The aqueous colloidal dispersion investigated here consists of short-range repulsive polystyrene–butylacrylate (PS/BA) particles (provided by BASF SE). The particle size is 85 nm in radius controlled by seeded emulsion polymerization. Acrylic acid was used as a surface functional comonomer of 2 wt% relative to the total monomer concentration.

Linear polyethylene oxide (PEO) has been added as a non-adsorbing polymer in order to induce attractive depletion interactions in the aqueous polymer dispersions. Different commercial grades (Merck Schuchardt OHG, Sigma Aldrich) with  $M_{\text{w}}$  between 4 and 400 kg mol<sup>−1</sup> have been used. The particular  $M_{\text{w}}$  values and corresponding radii of gyration,  $R_{\text{g}}$ , in water<sup>52</sup> are listed in Table 1. The width of the molecular weight distribution is  $M_{\text{w}}/M_{\text{n}} \approx 1.10$  according to the supplier. The  $c^*$  values are calculated as  $c^* = \frac{2.5}{[\eta]}$  where  $[\eta]$  is an intrinsic viscosity with the relation:  $[\eta] = 1.25 \times 10^{-4} M_{\text{w}}^{0.78}$  derived for PEO solutions in the range of  $10^4 < M_{\text{w}} < 10^7 \text{ g mol}^{-1}$ .<sup>53</sup>

According to Asakura–Oosawa<sup>54</sup> we have estimated the depletion interaction potential  $\psi_{\text{dep}}$  of two particles in contact for the different cases investigated here as:

**Table 1** Characteristic parameters of the PEO added as a depletion agent to the aqueous dispersion as well as of the linear polystyrene used for both microgel systems  $N = 11$  (M1) and 2.5 (M2). Values for two particle depletion interaction energy  $\Psi_{\text{dep}}/kT$  have been estimated for the used polymer concentrations  $c_p$  according to Asakura–Oosawa.<sup>54</sup> Polymer concentrations, for which fluidization was observed, are printed in bold italics. For the calculation of  $\Psi_{\text{dep}}$  a typical excluded volume of particles of  $\phi = 0.64$  was assumed, and the corresponding value for the true polymer concentration in the liquid phase was inserted in eqn (3). Note that in reality, at high particle loading  $\phi = 0.64$ , the corresponding depletion interaction energy is almost 4 to 5 times higher due to a so-called collective effect from the neighboring particles.<sup>55</sup>

Aqueous dispersion:

$M_w/\text{g mol}^{-1}$	$R_g/\text{nm}$	$R_g/R$	$c^*/\text{g l}^{-1}$	$-\Psi_{\text{dep}}/kT$		
				$c_p = 5 \text{ g l}^{-1}$	$c_p = 8 \text{ g l}^{-1}$	$c_p = 10 \text{ g l}^{-1}$
4000	2.5	0.030	310	<b>0.62</b>	1.03	1.3
10 000	4.2	0.049	152	<b>0.43</b>	<b>0.71</b>	0.86
20 000	6.3	0.074	88	<b>0.26</b>	<b>0.43</b>	0.55
35 000	8.7	0.102	57	<b>0.22</b>	0.36	0.42
400 000	36	0.424	8.5	0.043	0.076	0.086

Microgel system:

$N$	$M_w/\text{g mol}^{-1}$	$R_g/\text{nm}$	$R_g/R$	$c^*/\text{g l}^{-1}$	$-\Psi_{\text{dep}}/kT$		
					$c_p = 5 \text{ g l}^{-1}$	$c_p = 8 \text{ g l}^{-1}$	$c_p = 11 \text{ g l}^{-1}$
11	133 000	13.1	0.088	23.5	<b>0.22</b>	<b>0.35</b>	0.48
2.5	133 000	13.1	0.082	23.5	<b>0.24</b>	<b>0.34</b>	0.56

$$\frac{\Psi_{\text{dep}}}{kT} = -\frac{3}{2} \left( \frac{R}{R_g} \right) \phi_p \quad (3)$$

where  $\phi_p$  is the volume concentration of polymer in the liquid phase. The origin of depletion interaction is due to the osmotic pressure difference in the fluid phase and the gap between particles in which the non-adsorbing polymer is introduced. The calculation of  $\Psi_{\text{dep}}/kT$  according to eqn (3) at a particle loading of 0.64 is based on the free liquid phase and by the conversion of  $c_p$  in  $\text{g l}^{-1}$  to its volume fraction taking into account the volume occupied by the particles.

Highly concentrated dispersions including polymer dissolved in the continuous phase were prepared by a dialysis procedure. A dialysis membrane (Carl Roth GmbH, molecular weight cut off limit: 4000–6000  $\text{g mol}^{-1}$ ) filled with desired dispersion was immersed in a dialysis bath filled with an aqueous solution of 35 000  $\text{g mol}^{-1}$  of polyethylene oxide (PEO) at a concentration of 20% by weight. The high osmotic pressure of the PEO solution concentrates the dispersion to the desired particle volume fraction.

### Rheological characterization

**Rotational rheometry.** Steady and oscillatory shear measurements were performed using a strain-controlled ARES rheometer (TA Instruments) with a cone–plate geometry (radius 25 mm, 0.1002 radian angle). In steady shear experiments the shear rate was varied from 0.01 to 1000  $\text{s}^{-1}$ . Oscillatory shear experiments covered the frequency range from  $10^{-3}$  to 15 Hz and the strain was set to 0.01. Amplitude sweeps were performed in advance ensuring that linear viscoelastic fluid properties are probed under these conditions. A pre-shear test with a frequency of 1 Hz and a controlled strain at 4.5 was carried out for 500 seconds prior to all measurements to prepare a well-defined initial condition for the rheological characterization. The temperature was controlled by a fluid thermostat device at  $(20 \pm 0.1)^\circ\text{C}$ .

**Oscillatory squeeze flow.** The characterization of the linear viscoelastic response of the dispersions was extended to frequencies beyond 15 Hz using oscillatory squeeze flow via a Piezo Axial Vibrator (PAV) apparatus.<sup>56</sup> The samples were placed between two parallel, circular plates with a diameter of 20 mm and a separation of 20  $\mu\text{m}$ . The upper plate is constructed as a gas-tight lid and is tightly screwed to the base plate. The lower plate is driven through two pairs of piezoelectric actuators. By applying a sinusoidal voltage via a lock-in amplifier the plate oscillates around a mean position. Two further piezoelectric sensor pairs deliver the response signal. Measurements with the samples are compared to a measurement of the empty cell and the desired rheological quantities are calculated from the ratio of the output voltage with and without sample  $U/U_0$  and the corresponding phase shift  $\varphi - \varphi_0$ . This device covers the frequency range from 0.1– $10^3$  Hz. The temperature was controlled by a fluid thermostat device at  $(20 \pm 0.01)^\circ\text{C}$ .

### Dynamic light scattering (DLS)

**Particle sizing.** Dynamic light scattering experiments for particle sizing were performed on a standard light scattering instrument (ALV DLS/SLS-5000F) from ALV/Langen equipped with a SOSIP dual photomultiplier and employing a HeNe laser (JDS Uniphase) with a wave length  $\lambda = 633 \text{ nm}$  and a power output of 23 mW. Measured intensity autocorrelation functions  $g_T^{(2)}(q, \tau)$

$$g_T^{(2)}(q, \tau) = \frac{\langle I(q, t)I(q, t + \tau) \rangle_T}{\langle I(q, t) \rangle_T^2} \quad (4)$$

( $T$  denotes a time average;  $q$  is the scattering vector, eqn (6)) were converted into intermediate scattering functions  $f(q, \tau)$  using the Siegert relation<sup>57</sup> and analyzed via cumulant analysis.<sup>58</sup> The obtained diffusion coefficients were then converted into particle hydrodynamic radii via the Stokes–Einstein equation.<sup>57</sup> To

obtain accurate particle radii, aqueous dispersions were diluted to  $\phi < 10^{-4}$  and measurements of  $g_T^{(2)}(q, \tau)$  were taken over the full angular range from  $30^\circ$  to  $130^\circ$  in steps of  $5^\circ$  taking 10 measurements of 1 min duration per angle. The angular independence of the particle radii indicated the absence of particle aggregates as well as the narrowness of the size distribution. Averaging all measurements then provided hydrodynamic radii  $R_{h, H_2O}$  with a standard deviation of about 2%. Analogous analysis of swollen particle radii in the good solvent toluene gave much less accurate results ( $\pm 5\%$ ). As the swelling ratios  $Q$  determined from DLS via  $Q_{DLS} = (R_{h, Tol}/R_{h, H_2O})^3$  are thus much less accurate than those obtained via the phase behavior analysis and as it is uncertain whether the particle swelling in toluene is close enough to that in 2-EN, particle radii in toluene and  $Q_{DLS}$  were only used for first orientation when preparing samples for the phase behavior analysis and were not further used.

**Glass transition dynamics.** The full information about the particle dynamics of colloidal dispersions is contained in the intermediate scattering function  $f(q, \tau)$  which is defined as the normalized time correlation function of the  $q^{\text{th}}$  spatial Fourier component of fluctuations in the particle number density  $\rho(\vec{r}, t)$ ,

$$f(q, \tau) = \frac{\langle \delta\rho(\vec{q}, \tau) \delta\rho(\vec{q}, 0) \rangle}{\langle |\delta\rho(\vec{q}, 0)|^2 \rangle}; \quad q = |\vec{q}|; \quad (5a)$$

$$\delta\rho(\vec{q}, t) = \int \delta\rho(\vec{r}, t) \exp[i\vec{q} \cdot \vec{r}(t)] d\vec{r}, \quad (5b)$$

Here  $q$  denotes the scattering vector which is connected to the scattering angle  $\theta$  via

$$q = (4\pi n_D/\lambda) \sin(\theta/2) \quad (6)$$

Intermediate scattering functions in the glass transition range were determined on a custom-made dynamic light scattering instrument which has been described previously<sup>17,59</sup> employing a HeNe-Laser (JDS Uniphase) with  $\lambda = 633$  nm and an output power of 17 mW. Measured intensity autocorrelation functions  $g_T^{(2)}(q, \tau)$  were converted into intermediate scattering functions  $f(q, \tau)$  in three ways, depending on the degree of non-ergodicity of the sample dynamics using the intercept value  $g_T^{(2)}(q, 0)$  (averaged over a number of measurements—typically 3–5) as a criterion.

(i) For fully ergodic (=fluid) samples, indicated by  $g_T^{(2)}(q, 0) = 1.97$ – $1.9$ , measured  $g_T^{(2)}(q, \tau)$  were converted into  $f(q, \tau)$  as for dilute dispersions by using the usual Siegert relation.<sup>57</sup>

(ii) For fully non-ergodic (=glassy) samples, indicated by  $g_T^{(2)}(q, 0) < 1.6$ , the so-called Pusey–van Meegen (PvM) procedure<sup>60</sup> was used which assumes that the particles are localized in cages of their neighbors and can only perform small excursions about fixed equilibrium positions on the experimental time scale. Here the Siegert relation is replaced by

$$f(q, \tau) = 1 + (I_T/I_E) \{ [g_T^{(2)}(q, \tau) - g_T^{(2)}(q, 0) + 1]^{1/2} - 1 \} \quad (7)$$

$I_T$  is the time-averaged intensity which is automatically recorded during a particular experiment.  $I_E$  is the ensemble-averaged intensity which was determined from the photon counts accumulated while the sample is rotated for about 10 min with

a rotational frequency of about  $1/60$  s<sup>-1</sup>. Application of eqn (7) requires ideally an intercept  $g_T^{(2)}(q, 0) = 2$  which can be achieved to a good approximation by coupling the scattered light into a monomode fiber.<sup>59</sup>

(iii) For samples which are only partially ergodic (glass transition region) as there are fluid regions in the sample where some particles can escape their cage on the experimental time scale, the PvM procedure can no longer be applied.<sup>59,61</sup> Such samples typically have (average) intercept values between 1.9 and 1.6 as demonstrated previously.<sup>18</sup> In this case we apply the multispeckle approach.<sup>59,62</sup> Here the photomultiplier is replaced by a CCD camera which acts as a multidetector system and allows for monitoring a large number of intensity correlation functions simultaneously (in our case 300) for the same scattering vector  $q$ . These are then averaged (*cf.* eqn (3) of ref. 62) to obtain the ensemble averaged time correlation function  $g_E^{(2)}(q, \tau)$  which is then converted into  $f(q, \tau)$  by the use of the Siegert relation. Due to the recording frequency ( $50$  s<sup>-1</sup>) of the CCD camera, only delay times  $\tau > 20$  ms were accessible. To obtain  $f(q, \tau)$  over the full time range of  $10^{-7}$  s  $\leq \tau \leq 10^3$  s the multispeckle data were complemented by standard DLS experiments performed simultaneously<sup>17</sup> on the same sample volume and analyzed via the PvM method as described above (ii). The multispeckle data were then normalized to the DLS data in an overlap region  $1$  s  $\leq \tau \leq 10$  s.

Typical sampling times were  $1000\tau_{\text{max}}$  ( $\tau_{\text{max}}$  = longest delay time that was to be monitored) for ergodic samples (i) and 1 day for (partially) non-ergodic samples (ii and iii). Each measurement was repeated 3–5 times and averages were then taken.

### 3. Results and discussion

#### Microgel mixtures

The microgel system has been characterized by dynamic light scattering and in steady shear as well as in small amplitude oscillatory shear (SAOS) experiments particularly with respect to the effect of the small amount of larger particles introduced to suppress crystallization. Dynamic light scattering results for the mixed microgel system M1 are shown in Fig. 1a. Here the glass transition manifests itself in a non-vanishing long-time limit of the density autocorrelation function,  $f(q, \tau \rightarrow 0)$ , or the onset of a well-expressed plateau in a very narrow volume fraction range. To determine the glass transition volume fraction  $\phi_g$  we make use of the power law

$$\tau_\alpha = \tau_0(1 - \phi/\phi_g)^{-\gamma} \quad (8)$$

which has been predicted by the mode coupling theory<sup>24</sup> and which has been shown to describe the volume fraction dependence of the structural relaxation time,  $\tau_\alpha$ , in the neighborhood of a glass transition quite well.<sup>26,59</sup> The structural relaxation time values were read from the data in Fig. 1a according to the condition  $f(q, \tau_\alpha) = 0.5$  and are shown in the inset in the form of a rectification plot using the known exponent  $\gamma = 2.55$ . The intersection of the obtained straight line with the abscissa yields the glass transition volume fraction  $\phi_g = 0.585 \pm 0.008$ . The small shift of the glass transition to higher volume fractions as compared to the value of 0.58 for the monomodal system—even though barely outside of the experimental error—is

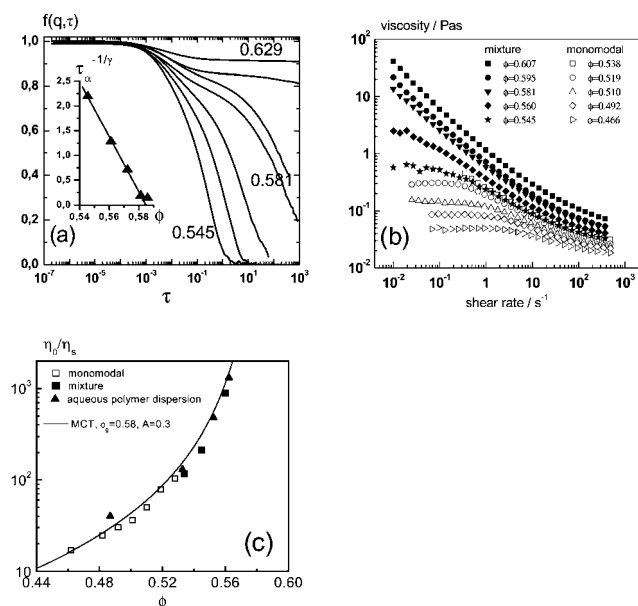


**Fig. 1** (a) Time evolution of the density autocorrelation function  $f(q, \tau)$  for the HS microgel mixture M1 ( $R_S = 144$  nm and  $R_L = 199$  nm,  $\Gamma = 0.722$  and  $N_1 = 11$ ) in the good, isorefractive solvent 2-ethylnaphthalene (2-EN) at volume fractions  $\phi = 0.545, 0.561, 0.572, 0.581, 0.586, 0.594$  and  $0.629$  (from left to right). Measurements were taken at a scattering vector  $qR_S = 3.96$  close to the main peak of the static structure factor. The inset shows the rectification plot of the MCT power law (eqn (8)) for the structural relaxation times  $\tau_\alpha$  used to determine the glass transition volume fraction of the mixture M1 as  $\phi_g = 0.585$ .  $\tau_\alpha$  was determined by the condition  $f(q, \tau_\alpha) = 0.5$ . (b) Steady shear viscosity as a function of shear rate for the monomodal microgel ( $R = 144$  nm, open symbols) and for the mixture M1 (closed symbols). (c) Relative zero shear viscosity against volume fraction for PS microgels (monomodality = open squares, bimodal (M1) = solid squares) and the aqueous dispersions (solid triangles). Prediction by the mode coupling theory (MCT) (eqn (9)) is shown as a solid line.

qualitatively consistent with the MCT for binary hard spheres<sup>63</sup> where such an effect has been predicted for  $\Gamma = 0.7$  and  $N = 11$  (corresponding to  $\phi_S/\phi \approx 0.8$  in Fig. 1 of ref. 63). The corresponding analysis for the mixture M2 yields  $\phi_g = 0.584 \pm 0.008$ , again qualitatively consistent with theory.

Fig. 1b shows the viscosity as a function of shear rate for the monomodal system with  $R_S = 144$  nm and mixture M1 ( $N = 11$ ) at different particle volume fractions. The fluid samples are identified by the finite zero-shear viscosity  $\eta_0$ , whereas the glassy state corresponds to a divergence of the viscosity at low shear rates.

The MCT predicts the divergence of the zero-shear viscosity with a power law

$$\eta_0/\eta_S = A(1 - \phi/\phi_g)^{-\gamma} \quad (9)$$

which is analogous to that of the structural relaxation time  $\tau_\alpha$  and which features the same critical scaling exponent  $\gamma$ .<sup>24</sup> Using eqn (9) with the known experimental HS value<sup>21,25,26</sup>  $\phi_g = 0.58$  and with the theoretical HS value  $\gamma = 2.55$  the experimental data for the monomodal system and the data points for the mixed system M1 appear to follow the same theoretical curve

with  $A = 0.3$ . A closer scrutiny *via* a rectification plot (not shown here) analogous to that for  $\tau_\alpha$  depicted in the inset of Fig. 1a verifies  $\phi_g = 0.58$  for the monomodal system while for the mixture M1 a slightly higher value of 0.585 is found. Even though this small difference is within the experimental error of the steady shear data, it is fully consistent with the DLS analysis for M1 where the same  $\phi_g$  value was obtained. A similar comparison for the monomodal system was not possible as the DLS value was not accessible due to the fast crystallization of these samples.

The linear viscoelastic moduli  $G'$  and  $G''$  have been obtained in the frequency range from  $10^{-3}$  Hz to  $10^3$  Hz. In Fig. 2 these data are shown as a function of Peclet number or reduced frequency  $Pe = 6\pi\eta_S R^3 \omega/kT$ . Here we use the number average HS radius due to the bimodality of the microgel system as<sup>16</sup>  $R = (R_1 + R_2 N)/(1 + N)$ .

The transition from the fluid to the glassy state shows up in a predominantly elastic material response ( $G' > G''$ ) and a non-vanishing zero-frequency storage modulus. These data can be analyzed in terms of the mode coupling scheme proposed by Fuchs and Cates<sup>30</sup> as described in Siebenbürger *et al.*<sup>32</sup> The density correlator  $\phi(t)$  is related to the memory function  $m(t)$  according to the following equations:

$$\partial_t \phi(t) + \Gamma \left\{ \phi(t) + \int_0^t d_t m(t-t') \partial_t \phi(t') \right\} = 0 \quad (10)$$

$$m(t) = \frac{\nu_1 \phi(t) + \nu_2 \phi^2(t)}{1 + (\dot{\gamma}t/\gamma_c)^2} \quad (11)$$

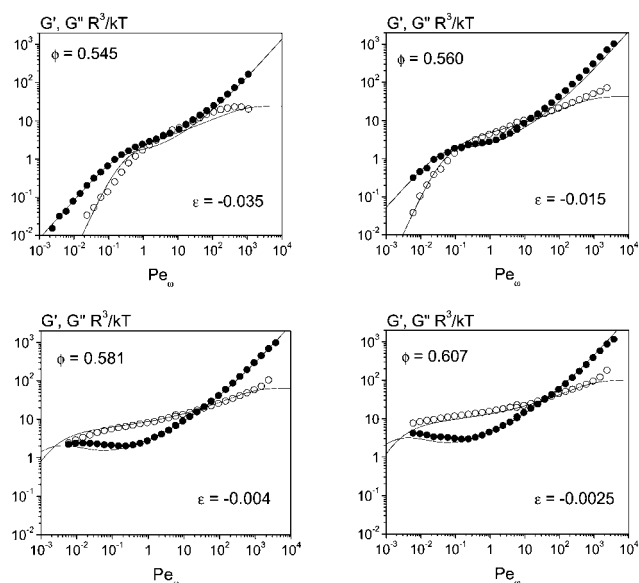


**Fig. 2** (a–d) Reduced storage modulus  $G' R/kT$  (open symbols) and loss modulus  $G'' R/kT$  (closed symbols) as a function of Peclet number for the microgel mixture M1 ( $N = 11$ ) without added polymer. The solid lines are fits of the MCT (eqn (10)–(13)) to the experimental data. Volume fractions are as indicated and the fit parameter  $\varepsilon = (\phi - \phi_g)/\phi_g$  denotes the relative distance from the glass transition.

with

$$\nu_1 = \nu_1^c + \varepsilon \frac{1 - f^c}{f^c} \quad (12)$$

The complex shear modulus  $G^* = G' + iG''$  is then given as:

$$G'(\omega) + iG''(\omega) = i\omega \int dt e^{-i\omega t} \nu_\sigma \phi^2(t)_{\dot{\gamma}=0} + i\omega \eta_\infty \quad (13)$$

where  $\nu_1^c = 0.828$ ,  $\nu_2 = 2$  and  $f^c = 0.293$  are fixed model parameters<sup>22</sup> and  $\varepsilon$ ,  $\nu_\sigma$ ,  $\Gamma$ ,  $\gamma_c$  and  $\eta_\infty$  are fitting parameters.

The values for these fitting parameters resulting for the microgel suspensions with different particle volume fractions are summarized in Table 2. The parameter  $\varepsilon = \frac{\phi - \phi_g}{\phi_g}$  is a reduced

volume fraction and  $\varepsilon = 0$  corresponds to the glass transition at  $\phi = \phi_g$ . The MCT for HS describes the linear viscoelastic properties of the microgel system very well and the small  $\varepsilon$  values at the highest volume fraction indicate the closeness to the glass transition. Fig. 3 displays the plateau modulus  $G_0$  and the longest relaxation time  $\lambda_{\max}$  from oscillatory shear experiments as a function of particle volume fraction. The latter quantity is defined as the inverse frequency  $\omega_c^{-1}$  at which  $G' = G''$ . The plateau modulus  $G_0$  is defined as the value of  $G'$  at the frequency at which  $G''$  exhibits a local minimum. The zero-shear viscosity (*cf.* Fig. 1c) and the longest relaxation time diverge as  $\phi$  approaches  $\phi_g$ , whereas  $G_0$  increases only weakly across the glass transition. The absolute values and also the weak concentration dependence for  $G_0$  agree well with older data for hard sphere systems.<sup>64</sup>

Thus, dynamic light scattering, small amplitude oscillatory shear and steady shear experiments consistently reveal that the microgel suspension behaves like an ideal hard sphere system and that the mixture of the slightly different particle sizes has no significant impact on the bulk rheological properties of the suspension except for a small, but noticeable shift of the glass transition to higher volume fractions in agreement with MCT predictions.<sup>63</sup> Similar results have been obtained for the mixture M2 with small to large particle number ratio  $N = 2.5$  (not shown).

### Re-entry behavior of microgel systems with weak attractive interactions

After having demonstrated for the pure binary microgel mixture M1 that rheology and dynamic light scattering yield consistent results on approaching the glass transition, we wanted to check whether this analogy in dynamical behaviour still holds when weak short-ranged attractions are introduced by the addition of free polymer. Here, the question of most interest was whether the

**Table 2** All parameters used in fitting of the MCT (eqn (10)–(13)) to the experimental data are summarized here for microgel suspension M1 with different particle volume fractions as shown in Fig. 2

$\phi$	$\varepsilon$	$\nu_\sigma$	$\Gamma$	$\gamma_c$	$\eta_\infty$
0.545	−0.035	24	140	120	0.8
0.560	−0.015	42	155	120	0.8
0.581	−0.0040	65	180	120	0.8
0.607	−0.0025	100	185	120	0.8

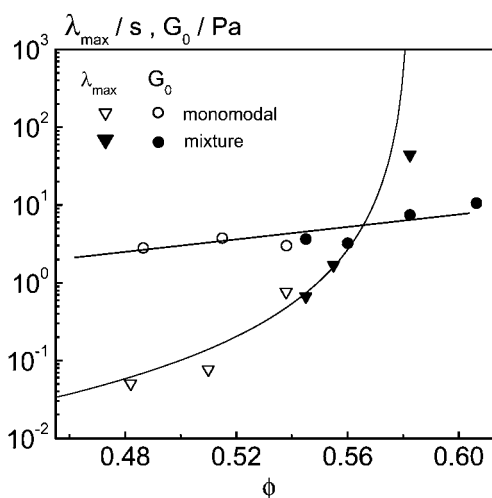


**Fig. 3** Maximum relaxation time,  $\lambda_{\max}$  (triangles), and plateau modulus  $G_0$  (circles) obtained from the frequency dependence of linear viscoelastic modulus,  $G'$  and  $G''$  for mono- and bimodal ( $\Gamma = 0.722$ ,  $N = 11$ ) PS microgel. The straight line is to guide the eye with respect to the  $G_0$  data and the curve is a fit of the functional form of eqn (9) to the  $\lambda_{\max}$  data with  $\phi_g = 0.58$ .

very strong re-entry effect that has been previously observed in a similar system<sup>18</sup> is expressed in an identical manner in the flow behaviour, thereby opening up a new access to prepare highly concentrating—yet freely flowing—dispersions. For this purpose linear PS was added to the mixed microgel suspensions as a non-adsorbing depletion agent at polymer concentrations  $c_p$  up to  $15 \text{ g l}^{-1}$ . The dynamics of the samples were investigated using steady and small amplitude oscillatory shear as well as dynamic light scattering. In the rheological experiments samples were classified as fluid, when a low shear plateau of the viscosity was observed in the accessible shear rate or frequency range, samples exhibiting a power-law dependence  $\eta \approx \dot{\gamma}^\alpha$  were identified to be in the glassy state and samples for which the  $\eta - \dot{\gamma}$  curves exhibit a curvature (in the log–log-plot) but no clear low shear plateau could be determined were termed to be in the transition state. In the DLS experiments a similar approach as used for the determination of the glass transition point of the pure binary mixture could not be generally followed here due to the extremely time consuming measuring times. Thus, a simpler and less time consuming, but less precise strategy was adopted. The distinction between the fluid and the glass was made on the basis of the average intercept values  $g_T^{(2)}(q, 0)$ . Samples with  $g_T^{(2)}(q, 0) > 1.9$  were considered as fluid, samples with  $g_T^{(2)}(q, 0) \leq 1.7$  as glassy and samples with intercepts in between were denoted as in the transition region. This allocation is consistent with previous observations for pure binary mixtures and was found to work decently well for colloid polymer mixtures in cases where both analysis strategies could be compared.<sup>18</sup> Only in a few cases the location of the glass transition point could be estimated by a rectification plot (*cf.* inset of Fig. 1a) with acceptable accuracy using two samples close enough to the transition line.

The resulting phase diagram is shown in Fig. 4. The results from rheology and DLS agree very well except for a small displacement of the reentry region to higher polymer concentrations in rheology as compared to DLS. This shift most likely

reflects the different experimental time scales of the two methods as compared to the time scale of sample dynamics, *i.e.* the different experimental time windows than can be accessed by DLS and rheology. As reported earlier<sup>18</sup> a large re-entry region with  $\phi_g \approx 0.68$  is found by both experimental probes. The phase behavior of both mixtures with  $N = 11$  and  $N = 2.5$  is very similar and apart from a slight shift along the  $\phi$ -axis the phase diagram coincides with that obtained by Eckert and Bartsch<sup>18</sup> as far as the repulsive branch of the glass line is concerned. For the attractive branch one finds a hint to a slight displacement to higher polymer concentrations. However, this is based on one securely extrapolated glass transition point from DLS data for M2. In the other cases sufficiently accurate DLS data could not be achieved, at least for M1 due to too fast crystallization in the neighborhood of the attractive glass line. Such an enhancement of crystallization close to the attractive arrest line has been observed and studied in detail at a volume fraction slightly below  $\phi_g$  for a similar attractive microgel mixture. However, the overall agreement between previously observed phase behavior and the results obtained for M1 and M2 indicates that a slight disturbance of an essentially monomodal particle size distribution due to the small fraction of slightly larger particles has no significant effect on the re-entry phenomenon. The slight shift in  $\phi$  compared to the previously investigated system originates in the different glass transition values of the binary mixtures studied

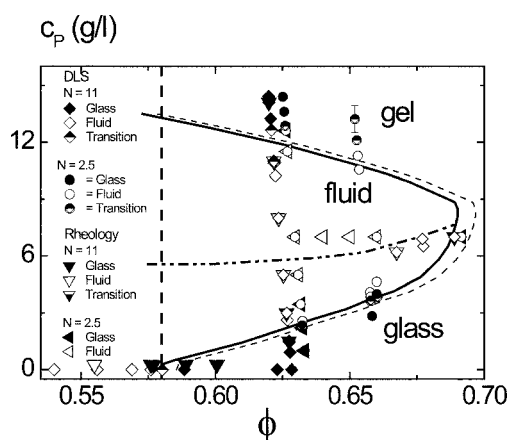


**Fig. 4** Re-entry phase diagram for the mixed microgel systems with  $N = 11$  (M1) and  $N = 2.5$  (M2) as indicated. Open symbols denote the fluid state, closed symbols denote glass state, half filled symbols mark the transition region where the state could not be unambiguously defined. Stars are transition points estimated by an extrapolation from relaxation times  $\tau_\alpha$  similar to Fig. 1a, inset (*cf.* text). For clarity the volume fractions for M1 have been multiplied by 0.99 (thus making the glass transition of this sample coincident with  $\phi_g = 0.58$ , the value for the one-component HS system). The solid line and the dash-dotted line indicate the glass transition line and the line of minimal structural relaxation time determined previously for a very similar microgel system for comparison. These lines were shifted along the  $\phi$ -axis to account for the different  $\phi_g = 0.595$  obtained in that study<sup>18</sup> and matched to the rescaled glass transition volume fraction of M1. The vertical dashed line indicates the location of the glass transition of that binary microgel mixture. The thin dashed line is the same glass transition line, only adjusted to match the glass transition of M2 ( $\phi_g = 0.584$ ). The difference of these two lines also serves to visualize the effect of an inaccuracy in the volume fraction scale for M1. If not explicitly indicated, errors are smaller than the symbol size.

here ( $\phi_g = 0.585$ ) and previously ( $\phi_g = 0.595$ ).<sup>18</sup> This difference is at present not understood, but it is clearly outside of the relative error in the volume fractions. It could be, in principle, related to the difference in size ratio of present ( $\Gamma = 0.83$ ) and previous ( $\Gamma = 0.722$ ) systems. While this possibility cannot be completely ruled out, it is not consistent with theoretical predictions.<sup>63,65</sup> While available theoretical predictions disagree in some details—MCT predicting even an decrease of the glass transition volume fraction,<sup>63</sup> *i.e.*  $\phi_g/\phi_{g,HS} < 1$  for  $\Gamma = 0.8$ , while the multicomponent self-consistent generalized Langevin equation theory of colloid dynamics predicts in contrast  $\phi_g/\phi_{g,HS} > 1$  for this size ratio, both agree in the respect that  $\phi_g/\phi_{g,HS}$  should be larger for  $\Gamma = 0.7$  than for  $\Gamma = 0.8$  which is in contradiction to our findings. In addition  $\phi_g/\phi_{g,HS} \approx 1.03$  as found for the previously studied system ( $\Gamma = 0.83$ ,  $\phi_S/\phi \approx 0.8$  and molar fraction  $x_S \approx 0.6$ ) is predicted consistently by both theories to occur only for size ratios  $\Gamma > 0.6$ . However, both theories have not yet been systematically tested against experimental data. Thus no final conclusions can be drawn on behalf of them. Another explanation would be a systematic error in the setting of the volume fraction scale as polydispersity effects on the values of the freezing volume fraction  $\phi_F$  have been neglected in our procedure to set the volume fraction scale. While this should not affect the present system due to its small polydispersity (as discussed above), the same is not necessarily true for the previously studied system which had a significantly higher polydispersity. Even though the origin of the discrepancies in the absolute values of the glass transition volume fractions of the pure binary mixtures cannot be conclusively explained at present, this obviously does not affect the phase behavior of the corresponding colloid-polymer mixtures as it is almost identical within the accuracy with which the location of the glass lines was determined after an appropriate matching of the volume fraction scales. The main message of Fig. 4 is that the large re-entry region first observed in the microscopic dynamics *via* DLS is recovered fully by the shear experiments probing macroscopic flow.

For a closer inspection of the rheological behavior of suspensions in the re-entry region of the phase diagram, we have done steady and oscillatory shear as well as the DLS experiments on a series of samples with constant particle volume fraction  $\phi$ , but various dissolved polymer concentrations  $c_p$ . Corresponding flow curves are shown in Fig. 5 and characteristic parameters from small amplitude oscillatory shear and DLS experiments are compared to low shear viscosity data in Fig. 6. Obviously, the weak attraction induced by the added polymer has a strong effect on the low shear viscosity, whereas the viscosity at high shear rates where hydrodynamic forces dominate remains essentially unchanged. At the highest and lowest polymer concentrations investigated the viscosity shows strict power-law behavior  $\eta \approx \dot{\gamma}^\alpha$  in the low shear regime but at intermediate polymer concentrations  $5 \text{ g l}^{-1} \leq c_p \leq 11 \text{ g l}^{-1}$  a distinct Newtonian low-shear plateau is observed indicating a fluid state. At a given shear rate of  $0.01 \text{ s}^{-1}$  the steady shear viscosity drops by a factor of 50 comparing the suspension with  $c_p = 0$  and  $8 \text{ g l}^{-1}$  (Fig. 6a). The re-entry phenomenon has a drastic effect on the low shear viscosity never observed before. The fluidization of the highly concentrated suspension also shows up in the linear viscoelastic moduli, the measured  $G'$  and  $G''$  data have been analyzed with the MCT according to eqn (10)–(13). In this hard sphere

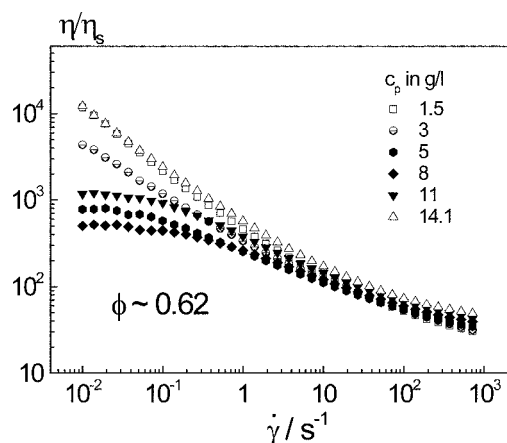


**Fig. 5** Reduced viscosity  $\eta/\eta_s$  versus shear rate for a series of microgel dispersions (M1,  $N = 11$ ) with similar particle volume fraction  $\phi \approx 0.62$  but different polymer concentrations. The closed symbols indicate the samples with fluid behavior and open symbols represent the glassy state.

mapping the fluidization manifests itself in a more negative value of the  $\varepsilon$  parameter (Fig. 6b), which can be interpreted as an increase in the distance to the glass transition or as an apparent reduction of the particle volume fraction.

All parameters  $\eta$ ,  $\varepsilon$  and  $\tau_\alpha$  exhibit a distinct minimum around  $c_p \approx 8 \text{ g l}^{-1}$ . The depth of this minimum is essentially the same for both microgel systems with  $N = 11$  and 2.5, *i.e.* the viscosity reduction in the re-entry regime is also not affected by the slight change in particle size distribution due to the added larger particles. At this point it should be noted that the viscosity reduction is not a consequence of osmotic de-swelling due to a reduced polymer concentration gradient across the particle boundary. Based on van't Hoff's equation for dilute ideal solutions  $\pi = c_p RT/M_w$  with the universal gas constant  $R$ , the osmotic pressure is estimated to be  $\pi \approx 220 \text{ Pa}$  in the concentration range where the viscosity minimum is observed. This value seems to be too small to induce a significant shrinkage of the microgel particles. For the previously investigated microgel system<sup>16</sup> this was further confirmed by preliminary small angle neutron scattering experiments where the particle form factor of

microgels was determined in dependence of the polymer concentration at a colloid volume fraction of 0.62 *via* contrast variation.<sup>66</sup> Instead the minimum is a generic feature of glass physics indicating the attraction-induced transition from a packing-driven glass to a bonding-driven glass *via* an intermittent fluid state.<sup>11–13</sup> Here the melting of the initial packing-driven glass results from the creation of free volume *via* attraction-induced transient particle bonds. On increase of the attraction strength the amount of bonds increases such that the dynamics eventually slows down again, thus creating the relaxation time (and viscosity) minimum, until the dispersion on further increase of attraction freezes into another glassy state—the bonding-driven glass. The variation of flow curves with increasing particle volume fraction but at a fixed polymer concentration  $c_p \approx 7 \text{ g l}^{-1}$  corresponding to the viscosity minimum for  $\phi \approx 0.63$  is shown in Fig. 7. The low shear viscosity increases by about a factor of 10 at  $\dot{\gamma} = 0.01 \text{ s}^{-1}$  already at  $\phi = 0.69$ ,  $\tau_\alpha = 10^4 \text{ s}$  is found. Accordingly, the Newtonian plateau is expected to occur for  $\dot{\gamma} \approx 10^{-4}$  to  $10^{-3} \text{ s}^{-1}$  and these systems are

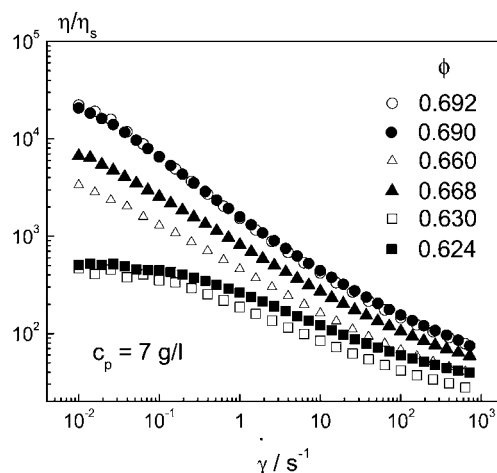


**Fig. 7** Viscosity as a function of shear rate for different particle concentrations  $\phi$  but constant polymer concentration  $c_p \approx 7 \text{ g l}^{-1}$ ,  $N = 11$  (M1, closed symbols),  $N = 2.5$  (M2, open symbols).

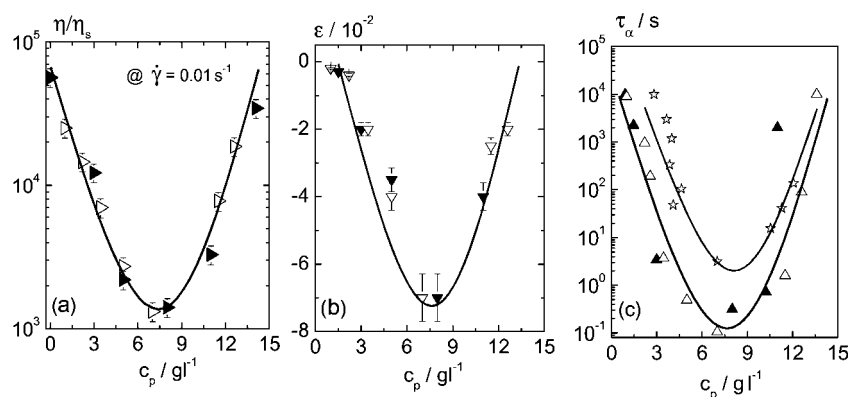


**Fig. 6** (a) Low shear viscosity  $\eta$  determined at  $\dot{\gamma} = 0.01 \text{ s}^{-1}$ , (b) parameter  $\varepsilon$  from a fit of MCT equations to small amplitude oscillatory shear data and (c) structural relaxation time  $\tau_\alpha$  from DLS as a function of polymer concentrations  $c_p$  for microgel suspensions M1 with  $N = 11$  (closed triangles) and M2 with  $N = 2.5$  (open triangles) at  $\phi \approx 0.63$  as well as for M2 at  $\phi \approx 0.66$  (open stars). Lines are for visual guidance.

presumably in the fluid state. This is further confirmed by negative  $\varepsilon$  values obtained when fitting of the MCT to the experimental  $G'$  and  $G''$  data, for  $\phi = 0.66$ ,  $\varepsilon = -0.4$  and for  $\phi = 0.69$ ,  $\varepsilon = -0.02$  is found.

### Re-entry phenomenon in aqueous polymer dispersions

A styrene-butylacrylate latex electrosterically stabilized by copolymerization of acrylic acid has been used to study the re-entry phenomenon for the class of aqueous dispersions. This latex essentially behaves like a hard sphere system as confirmed by the divergence of the relative zero-shear viscosity as the data included in Fig. 1c demonstrate. A fit of eqn (9) to the  $\eta/\eta_s$  data yields  $\phi_g = 0.58 \pm 0.005$ .

PEO has been used as a non-adsorbing depletion agent and the fluidization due to the added polymer is directly visible in the images of portions of suspension with different  $c_p$  placed on a glass plate shown in Fig. 8. The fluid sample spreads out on the plate whereas the glassy suspensions remain their shape. PEO molecular weight has been varied between  $M_w = 4000$  g mol<sup>-1</sup> and 400 000 g mol<sup>-1</sup> corresponding to a variation of  $R_g/R$  between 0.03 and 0.424. Typically  $\Psi_{\text{dep}}/kT$  is on the order of 0.1–1; the corresponding data are summarized in Table 1.

Fluid states were observed for PEO molecular weight 4000 g mol<sup>-1</sup>  $\leq M_w \leq 35$  000 g mol<sup>-1</sup> and  $c_p = 5$  g l<sup>-1</sup>. For  $M_w = 10$  000 g mol<sup>-1</sup> and 20 000 g mol<sup>-1</sup> a viscosity reduction is also found for  $c_p = 8$  g l<sup>-1</sup> but not at a higher polymer concentration. No significant change in viscosity was observed upon addition of PEO with  $M_w = 400$  000 g mol<sup>-1</sup>. The change in the flow curves with the concentration of added PEO ( $M_w = 10$  000 g mol<sup>-1</sup>) is shown in Fig. 9a for a particle volume fraction  $\phi = 0.644$ . Similar to the microgel case the introduction of weak depletion attraction leads to a sharp drop in the low shear viscosity by almost two orders of magnitude whereas high shear viscosity exhibits a weak monotonic increase with increasing  $c_p$  roughly by a factor of two. The variation of the reduced viscosity at a fixed shear rate is displayed in Fig. 9b.

Obviously, a pronounced viscosity minimum is reached at a polymer concentration  $c_p \approx 8$  g l<sup>-1</sup>. Fig. 10 displays the dependence of the low shear viscosity taken at a constant shear rate  $\dot{\gamma} = 0.01$  s<sup>-1</sup> and particle loading  $\phi = 0.644$  as a function of  $M_w$  of the added PEO expressed here in terms of  $R_g/R$ . At a fixed  $c_p = 5$  g l<sup>-1</sup> this low shear viscosity varies within a factor of three but there is no clear trend as  $M_w$  is varied. This may be due to the fact that increasing  $M_w$  corresponds to an increase in the range of attractive interactions but also to a decrease of the interaction strength. Presumably, these two phenomena have an opposite effect on fluidization. The observed viscosity variation is small compared to the drastic drop of low shear viscosity relative to the pure dispersion demonstrating that the re-entry phenomenon



**Fig. 8** Texture of aqueous dispersion without PEO (left, glassy) and with added PEO ( $M_w = 4000$  g mol<sup>-1</sup>,  $c_p = 5$  g l<sup>-1</sup> (middle, fluid) and  $c_p = 10$  g l<sup>-1</sup> (right, attractive glass) at  $\phi = 0.64$ .

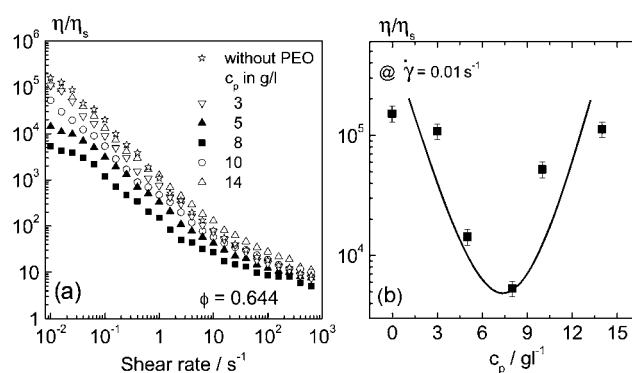


**Fig. 9** (a) Reduced viscosity  $\eta/\eta_s$  versus shear rate for a series of acrylate dispersions with similar particle volume fraction  $\phi \approx 0.644$  but different PEO ( $M_w = 10$  000 g mol<sup>-1</sup>) concentrations as indicated in the legend, (b) reduced low shear viscosity  $\eta/\eta_s$  determined at  $\dot{\gamma} = 0.01$  s<sup>-1</sup> as a function of added PEO concentration  $c_p$ . The line is for visual guidance. The closed symbols indicate the samples with fluid behavior and open symbols represent the glassy state.

provides a robust strategy to produce highly concentrated colloidal dispersions. It should be noted that polymer concentrations  $c_p$  are expressed relative to the total volume of the dispersion, but even if the excluded volume of the particles is taken into account the polymer concentration for the samples with minimum viscosity is far below  $c_p^*$ .

Finally, we set this viscosity reduction route in contrast to the classical strategy, *i.e.* a broad multimodal particle size distribution. Fig. 11 shows the flow curves for the P(S-BA) latex system with and without added polymer in comparison with that for the commercial polymer dispersion Acronal V215 (BASF SE) adjusted to the same particle volume fraction  $\phi$ . The particle size distribution of the latter dispersion is very similar to that of sample M2 described in ref. 10 and particle radii cover the range from 70 to 350 nm. Obviously, the viscosity reduction achieved through the re-entry phenomenon is close to that resulting from a broad particle size distribution. This demonstrates that the introduction of weak attractive particle interactions is a competitive strategy to make freely flowing but highly concentrated dispersions.

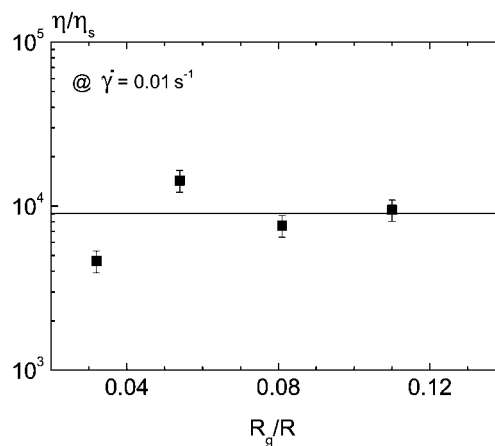


**Fig. 10** Reduced low shear viscosity  $\eta/\eta_s$  determined at  $\dot{\gamma} = 0.01$  s<sup>-1</sup> for the acrylate dispersion with  $\phi = 0.644$  as a function of size ratio of PEO to colloid at  $c_p = 5$  g l<sup>-1</sup> (closed symbols).

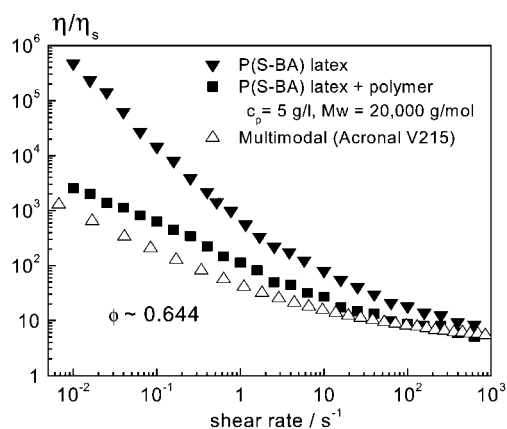


**Fig. 11** Comparison of flow curves for dispersions fluidized due to weak attractive depletion interactions and dispersions with a broad multimodal size distribution.

#### 4. Conclusion

Dense colloidal dispersions exhibit fluid states due to weak attractive interactions among particles even at particle volume fractions far above the colloidal glass transition. This so-called re-entry phenomenon opens up a new route to manufacture highly concentrated, freely flowing dispersions. Here we have studied the rheological properties of two model dispersions in the dense, fluid state: PS-microgel particles suspended in an isorefractive organic solvent and PS/BA particles with short range repulsive interactions dispersed in water. The former system is transparent enough to allow for dynamic light scattering experiments to study particle dynamics, the latter is close to technical polymer latex systems. Both systems essentially behave like hard spheres, their zero-shear viscosity diverges around  $\phi = 0.58$ , linear viscoelastic behavior is well-described by the mode coupling theory and the absolute values of the plateau moduli are close to those reported for other hard sphere systems. Fluidization was achieved by introducing weak depletion attraction among particles *via* addition of non-adsorbing polymers to the continuous phase, PS in the case of the microgel suspension and PEO in the case of the aqueous dispersion. Fluid states were observed up to  $\phi \approx 0.69$  for the microgel and up to  $\phi \approx 0.644$  for the aqueous system. At a given particle loading a minimum viscosity was achieved at polymer concentrations  $c_p \approx 8 \text{ g l}^{-1}$  below  $c_p^*$ . In the case of the aqueous dispersion fluidization was observed for a broad range of polymer molecular weights  $M_w$  corresponding to  $R_g/R$  ratios between 0.03 and 0.10 and the respective viscosity minimum did not vary systematically with  $M_w$ .

The weak dependence on added polymer molecular weight suggests that this strategy is robust and may be easily introduced to technical large scale emulsion polymerization processes. The fraction of monomers polymerized in the aqueous phase and their degree of polymerization have to be controlled by appropriate monomer feed and pH adjustment during polymerization and chemical stripping, such that the polymer chains required to induce the re-entry fluidization effect are formed *in situ*. Finally, the robust nature of the viscosity reduction effect against variation of  $R_g/R$  poses the question, whether synergistic effects occur when both strategies are combined and weak attractive

interactions are introduced to dispersions with broad particle size distributions. This topic will be addressed in our subsequent research activities.

#### Acknowledgements

We thank BASF SE for donating the styrene-butylacrylate model latex and the commercial dispersion Acronal V215. H. Moschallski is thanked for the synthesis of the microgel particles. The financial support by German Research Foundation DFG grant WI 3138/4-2 and BA 1619/1-2 is gratefully acknowledged.

#### References

- 1 P. C. Hiemenz and R. Rajagopalan, in *Principles of Colloid and Surface Chemistry*, Dekker, New York, 3rd edn, 1997.
- 2 D. J. Irvine, A. Stachowiak and S. Jain, *Mater. Sci. Forum*, 2003, **426**, 3213–3218.
- 3 Y. A. Vlasov, N. Yao and D. J. Norris, *Adv. Mater.*, 1999, **11**, 165–169.
- 4 G. M. Gratson, X. Mingjie and J. A. Lewis, *Nature*, 2004, **428**, 386–389.
- 5 J. A. Lewis, *J. Am. Ceram. Soc.*, 2000, **83**, 2341–2359.
- 6 A. Terray, J. Oakey and D. W. M. Marr, *Science*, 2002, **296**, 1841–1844.
- 7 R. J. Farris, *J. Rheol.*, 1968, **12**, 281–301.
- 8 A. T. J. M. Wouterson and C. G. de Kruif, *J. Chem. Phys.*, 1991, **94**, 5739–5749.
- 9 B. Dames and N. Willenbacher, *Rheol. Acta*, 2001, **40**, 434–440.
- 10 N. Willenbacher, L. Börger, D. Urban and L. Varela de la Rosa, *Adhes. Sealants*, 2003, **10**(9), 26–35.
- 11 L. Fabbian, W. Gotze, F. Sciortino, P. Tartaglia and F. Thiery, *Phys. Rev. E: Stat. Phys., Plasmas, Fluids, Relat. Interdiscip. Top.*, 1999, **59**, R1347–R1350.
- 12 L. Fabbian, W. Gotze, F. Sciortino, P. Tartaglia and F. Thiery, *Phys. Rev. E: Stat. Phys., Plasmas, Fluids, Relat. Interdiscip. Top.*, 1999, **60**, 2430.
- 13 K. Dawson, G. Foffi, M. Fuchs, W. Götze, F. Sciortino, M. Sperl, P. Tartaglia, T. Voigtmann and E. Zaccarelli, *Phys. Rev. E: Stat. Phys., Plasmas, Fluids, Relat. Interdiscip. Top.*, 2001, **63**, 011401.
- 14 K. N. Pham, A. M. Puertas, J. Bergenholtz, S. U. Egelhaaf, A. Moussaïd, P. N. Pusey, A. B. Schofield, M. E. Cates, M. Fuchs and W. C. K. Poon, *Science*, 2002, **296**, 104–106.
- 15 K. N. Pham, S. U. Egelhaaf, P. N. Pusey and W. C. K. Poon, *Phys. Rev. E: Stat., Nonlinear, Soft Matter Phys.*, 2004, **69**, 011503.
- 16 T. Eckert and E. Bartsch, *Phys. Rev. Lett.*, 2002, **89**, 125701.
- 17 T. Eckert and E. Bartsch, *Faraday Discuss.*, 2003, **123**, 51.
- 18 T. Eckert and E. Bartsch, *J. Phys.: Condens. Matter*, 2004, **16**, S4937.
- 19 S. A. Shah, Y. L. Chen, K. S. Schweizer and C. F. Zukoski, *J. Chem. Phys.*, 2003, **118**, 3350.
- 20 S. A. Shah, Y. L. Chen, K. S. Schweizer and C. F. Zukoski, *J. Chem. Phys.*, 2003, **119**, 8747.
- 21 P. N. Pusey and W. van Meegen, *Nature*, 1986, **320**, 340–342.
- 22 A. J. Liu and S. R. Nagel, *Nature*, 1998, **6706**, 21–22.
- 23 S. P. Meeker, W. C. K. Poon and P. N. Pusey, *Phys. Rev. E: Stat. Phys., Plasmas, Fluids, Relat. Interdiscip. Top.*, 1997, **55**, 5718.
- 24 W. Götze, in *Liquids, Freezing and Glass Transition*, North-Holland, Amsterdam, 1991.
- 25 W. Van Meegen and P. N. Pusey, *Phys. Rev. A: At., Mol., Opt. Phys.*, 1991, **43**(10), 5429–5441.
- 26 W. Van Meegen and S. M. Underwood, *Phys. Rev. E: Stat. Phys., Plasmas, Fluids, Relat. Interdiscip. Top.*, 1994, **49**(5), 4206–4220.
- 27 J. L. Barrat, W. Götze and A. Latz, *J. Phys.: Condens. Matter*, 1989, **1**, 7163–7170.
- 28 G. Nägele and J. Bergenholtz, *J. Chem. Phys.*, 1998, **108**(23), 9893–9904.
- 29 M. Fuchs and M. E. Cates, *Phys. Rev. Lett.*, 2002, **89**, 2483041–2483044.
- 30 M. Fuchs and M. E. Cates, *Faraday Discuss.*, 2003, **123**, 267.
- 31 M. Fuchs and M. Ballauff, *J. Chem. Phys.*, 2005, **122**, 094707.
- 32 M. Siebenbürger, M. Fuchs, H. Winter and M. Ballauff, *J. Rheol.*, 2009, **53**, 707.

- 33 J. Bergenholtz and M. Fuchs, *Phys. Rev. E: Stat. Phys., Plasmas, Fluids, Relat. Interdiscip. Top.*, 1999, **59**, 5706–5715.
- 34 V. Gopalakrishnan and C. F. Zukoski, *J. Rheol.*, 2004, **48**(6), 1321–1344.
- 35 L. N. Krishnamurthy and N. J. Wagner, *J. Rheol.*, 2005, **49**(3), 475–499.
- 36 K. N. Pham, G. Petekidis, D. Vlassopoulos, S. U. Egelhaaf, W. C. K. Poon and P. N. Pusey, *J. Rheol.*, 2008, **52**(2), 649–676.
- 37 V. Tohver, J. E. Smay, A. Braem, P. V. Braun and J. A. Lewis, *Proc. Natl. Acad. Sci. U. S. A.*, 2001, **98**(16), 8950–8954.
- 38 T. F. Tadros, *Adv. Colloid Interface Sci.*, 1996, **68**, 97.
- 39 R. Tuinier, J. Rieger and C. G. de Kruijff, *Adv. Colloid Interface Sci.*, 2003, **103**, 1.
- 40 J. S. Vesaratchanon, K. Takamura and N. Willenbacher, *J. Colloid Interface Sci.*, 2010, **345**, 214–221.
- 41 E. Bartsch, T. Eckert, C. Pies and H. Sillescu, *J. Non-Cryst. Solids*, 2002, **307**, 802–811.
- 42 S. E. Paulin and B. J. Ackerson, *Phys. Rev. Lett.*, 1990, **64**, 2663–2666.
- 43 W. G. Hoover and F. H. Ree, *J. Chem. Phys.*, 1968, **49**, 3609–3617.
- 44 H. Senff and W. Richtering, *J. Chem. Phys.*, 1999, **111**, 1705–1711.
- 45 W. G. Hoover, S. G. Gray and K. W. Johnson, *J. Chem. Phys.*, 1971, **55**, 1128–1136.
- 46 R. Agrawal and D. A. Kofke, *Mol. Phys.*, 1995, **85**, 23–42.
- 47 P. G. Bolhuis and D. A. Kofke, *Phys. Rev. E: Stat. Phys., Plasmas, Fluids, Relat. Interdiscip. Top.*, 1996, **54**, 634–643.
- 48 M. Fasolo and P. Sollich, *Phys. Rev. E: Stat., Nonlinear, Soft Matter Phys.*, 2004, **70**, 041410.
- 49 C. Urban and P. Schurtenberger, *J. Colloid Interface Sci.*, 1998, **207**, 150–158.
- 50 L. B. Aberle, P. Hulstede, S. Wiegand, W. Schroer and W. Staude, *Appl. Opt.*, 1998, **37**, 6511–6524.
- 51 E. Lange, J. B. Caballero, A. M. Puertas and M. Fuchs, *J. Chem. Phys.*, 2009, **130**, 174903.
- 52 S. Kawaguchi, G. Imai, J. Suzuki, A. Miyahara, T. Kitano and K. Ito, *Polymer*, 1997, **38**, 2885–2891.
- 53 F. E. Bailey, J. L. Kucera and L. G. Imhof, *J. Polym. Sci.*, 1958, **32**, 517–518.
- 54 S. Asakura and F. Oosawa, *J. Polym. Sci.*, 1958, **33**, 183.
- 55 M. Dijkstra, R. v. Roij and R. Evans, *Phys. Rev. E: Stat. Phys., Plasmas, Fluids, Relat. Interdiscip. Top.*, 1999, **59**, 5744–5771.
- 56 J. J. Crassous, R. Régisser, M. Ballauff and N. Willenbacher, *J. Rheol.*, 2005, **49**, 851–864.
- 57 B. Chu, *Laser Light Scattering*, Academic Press, Boston, 1991.
- 58 D. E. Koppel, *J. Chem. Phys.*, 1972, **57**, 4814–4860.
- 59 E. Bartsch, V. Frenz, J. Baschnagel, W. Schärfl and H. Sillescu, *J. Chem. Phys.*, 1997, **106**, 3743–3756.
- 60 P. N. Pusey and W. van Megen, *Physica A*, 1989, **157**, 705–741.
- 61 E. Bartsch, V. Frenz, S. Kirsch, W. Schärfl and H. Sillescu, *Prog. Colloid Polym. Sci.*, 1997, **40**, 104.
- 62 S. Kirsch, V. Frenz, W. Schärfl, E. Bartsch and H. Sillescu, *J. Chem. Phys.*, 1996, **104**, 1758–1761.
- 63 W. Götze and T. Voigtmann, *Phys. Rev. E: Stat., Nonlinear, Soft Matter Phys.*, 2003, **67**, 021502.
- 64 T. G. Mason and D. A. Weitz, *Phys. Rev. Lett.*, 1995, **75**, 2770–2773.
- 65 R. Juarez-Maldonado and M. Medina-Noyola, *Phys. Rev. E: Stat., Nonlinear, Soft Matter Phys.*, 2008, **77**, 051503.
- 66 J. Othegraven, T. Eckert, E. Bartsch and P. Lindner, unpublished data